Advances in Research

Volume 25, Issue 6, Page 381-391, 2024; Article no.AIR.128454
ISSN: 2348-0394, NLM ID: 101666096

An Advanced Spherical Bearing Model with FEA Analysis

Boxiong Hou [a*]

[a] *School of Civil and Transportation, North China University of Water Resources and Electric Power, Zhengzhou-450045, Henan, China.*

Author's contribution

The sole author designed, analysed, interpreted and prepared the manuscript.

Article Information

DOI: https://doi.org/10.9734/air/2024/v25i61211

Open Peer Review History:
This journal follows the Advanced Open Peer Review policy. Identity of the Reviewers, Editor(s) and additional Reviewers, peer review comments, different versions of the manuscript, comments of the editors, etc are available here: https://www.sdiarticle5.com/review-history/128454

Short Communication

Received: 15/10/2024
Accepted: 19/12/2024
Published: 21/12/2024

ABSTRACT

The mechanical properties of spherical bearing have a direct influence on the seismic performance of bridge construction. Aiming at QZ12500GD spherical bearing, Abaqus finite element analysis software was used for modeling and analysis, and vertical pressure, horizontal thrust and vertical tension were analyzed to study the deformation and stress of the bearing. The model parameters and modeling method of spherical bearing in finite element software analysis are obtained. The analysis results show that this kind of bearing form has good deformation and bearing capacity under the design bearing capacity, and meets the design requirements.

Keywords: Spherical bearing; stress; strain; finite element analysis.

1. INTRODUCTION

The painful lessons of previous earthquakes show that bridge is an important part of lifeline engineering, once it is seriously damaged in the earthquake, it will cause huge economic and social losses. Since the Wenchuan earthquake in 2008, more and more attention has been paid to

**Corresponding author: E-mail: 1599423348@qq.com;*

Cite as: *Hou, Boxiong. 2024. "An Advanced Spherical Bearing Model With FEA Analysis". Advances in Research 25 (6):381-91. https://doi.org/10.9734/air/2024/v25i61211.*

the aseismic problem of bridge, and the aseismic problem of support is an important part of bridge aseismic problem(Adamov et al. 2022).

Spherical bearings are one of the most widely used forms of bearings at present. Spherical bearings are provided with spherical friction pairs to make the bearings rotate flexibly(Ghalamchi et al. 2016). After overcoming the sliding friction between spherical crown steel plate and spherical polytetrafluoroethylene plate, the bearings rotate immediately, and their rotational torque is independent of the rotation Angle. It makes the force of the structure more reasonable and protects the safety of the whole structure(Ciubotariu 2016). It not only has the characteristics of large bearing capacity and large displacement, but also can better adapt to the needs of large rotation Angle of the support, so it is widely used in highway Bridges, municipal Bridges and rail transit Bridges.

At present, there are few examples of spherical bearings analyzed by using finite element software. In this paper, large-scale finite element analysis software Abaqus is used for analysis, a finite element model is established to test the mechanical performance of QZ12500GD seismic spherical bearings under design loads, and a modeling and analysis method using Abaqus is explored. And investigate whether it can meet the requirements of practical engineering use(McErlain et al. 2011).

2. BASIC STRUCTURE OF BEARING

In this paper, QZ12500GD seismic spherical bearing is analyzed as shown in Fig. 1.

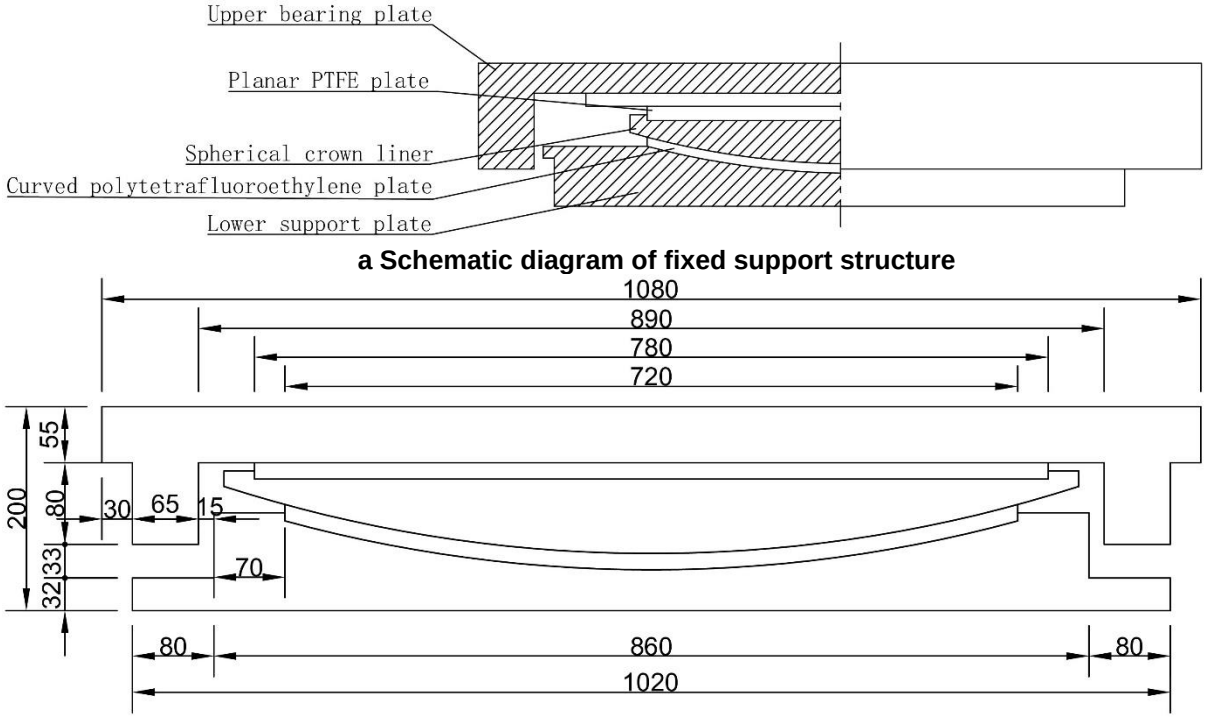

a Schematic diagram of fixed support structure

b Bearing size (mm)

Fig. 1. QZ12500GD seismic spherical bearing

3. BEARING FINITE ELEMENT MODEL

3.1 Finite Element Model

Three-dimensional geometric models of upper and lower support plates, spherical crown lining plates and tetrafluoroidal plates were established in Abaqus finite element software and assembled. The dimensions of each component were established according to Fig. 1b. The overall division element type of the support is basically C3D8R, eight-node linear hexahedron element, reduction integral, hourglass control, and the mesh length is 20mm, with a total of 17214 units and 30791 nodes. The model and grid division after the support assembly are shown in Fig. 2.

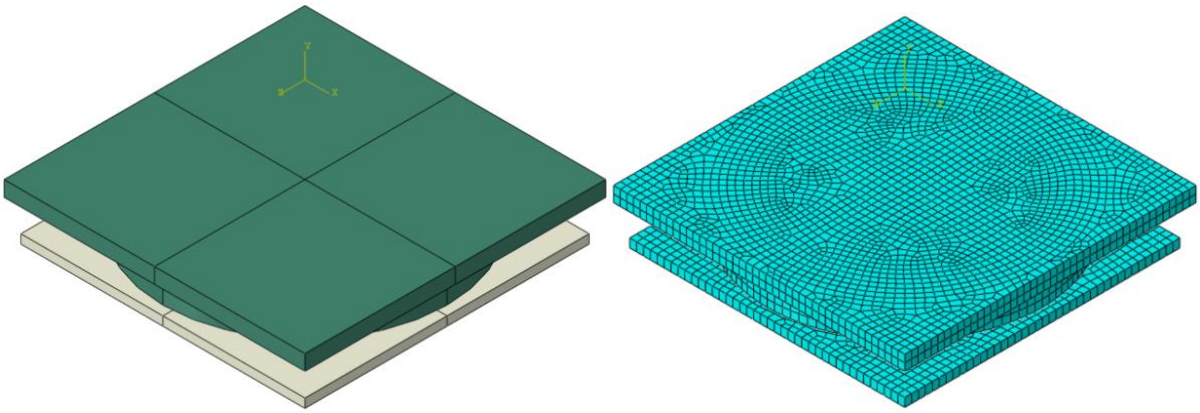

a Global model **b Meshing diagram**

Fig. 2. Finite Element Model of Seismic Spherical Bearing

3.2 Material Parameters

Table 1. The features of bearing material

Material	Elastic modulus/×10^9Pa	Poisson's ratio	Density/(kg·m^{-3})
Q235	200	0.3	7850
titanium alloy	96	0.36	4620
polyethylene	1.1	0.42	950

The upper and lower bearing plates of the bearing are made of Q235, the spherical cap liner is made of titanium alloy, and the PTFE plate is made of polyethylene. See Table 1 for specific parameters of each material.

4. FINITE ELEMENT ANALYSIS OF BEARING

In order to analyze and test the stress state of each component of the bearing and ensure the reliability of the bearing, the finite element analysis is carried out on the main load-bearing components of the bearing, focusing on the stress magnitude and distribution of its spherical lower seat plate, PTFE slide plate and spherical cap liner (Shah et al. 2016). The main contents include: static analysis, bearing modal analysis and dynamic analysis.

4.1 Static Analysis

4.1.1 Vertical pressure simulation

In order to simulate the test conditions of the bearing, a surface load is applied to the upper surface of the bearing, and the load is applied to 1.5 times the design bearing capacity (18750kN) step by step(Ahmed et al. 2024). The center point of the top surface of the upper bearing plate is selected for vertical displacement analysis, and the radial deformation of the bushing base of the lower bearing plate is analyzed, and the load-deformation curve can be obtained as shown in Fig. 3. There is a linear relationship between load and deformation (Desavale et al. 2014). When the maximum load is 18750kN, the maximum vertical deformation is 0.67mm, and the compression deformation is not more than 1% of the total height of the bearing. The maximum radial deformation of the lower bearing plate bushing base is 0.014mm, which is not more than 0.5% of the radial length, and meets the design requirements(Wang et al. 2011).

The result of extracting Abaqus partial stress is shown in Fig. 4. As can be seen from the figure, under the action of 1.5 times the design load, the maximum Mises stress is 106.2MPa, and all materials are in elastic state, which also reflects the correctness of the linear change of load-deformation curve and meets the design requirements(Xue et al. 2018).

4.1.2 Horizontal thrust simulation

In order to simulate the actual stress of the test, it is necessary to apply a load of 12500kN on the upper surface of the bearing, and apply it to the side of the upper bearing plate step by step to 1.2 times the horizontal design bearing capacity (1500 kN), and select the radial deformation

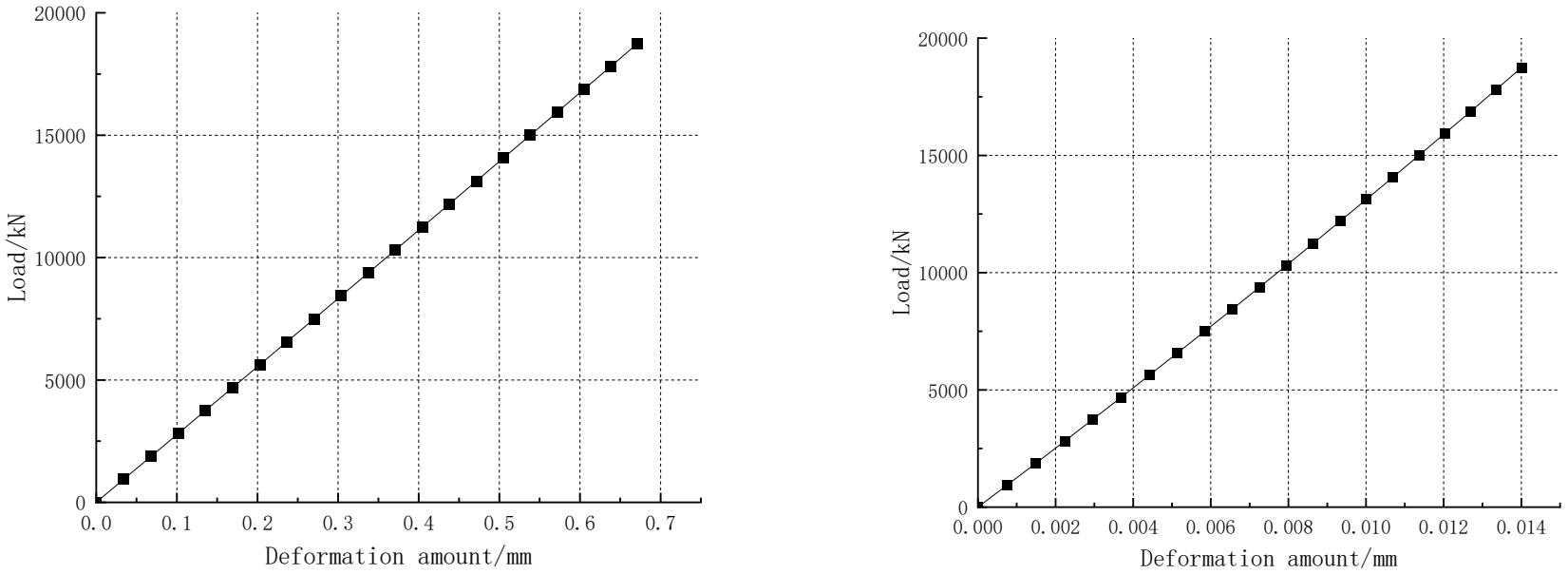

a Load vertical deformation relation curve b Load radial deformation relation curve

Fig. 3. Load-deformation relation curve

of the spherical cap liner to analyze (Mohamed Anwar et al. 2024). There is a linear relationship between load and deformation. When the maximum load is 1500kN, the maximum deformation in the horizontal direction is 0.72 mm. The results of extracting partial stress and displacement of Abaqus are shown in Figs. 5 and 6(Harris & Kotzalas 2006).

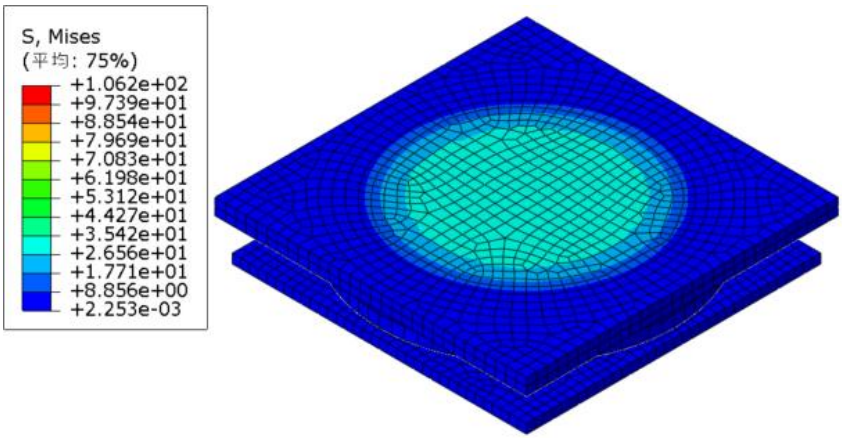

Fig. 4. Mises stress cloud

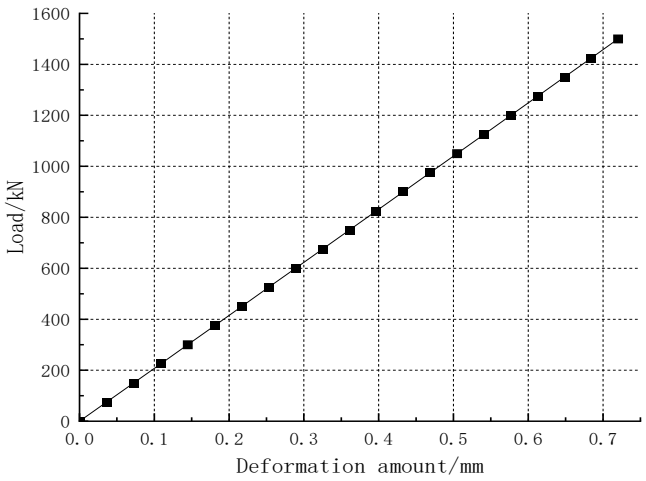

Fig. 5. Load radial deformation relation curve

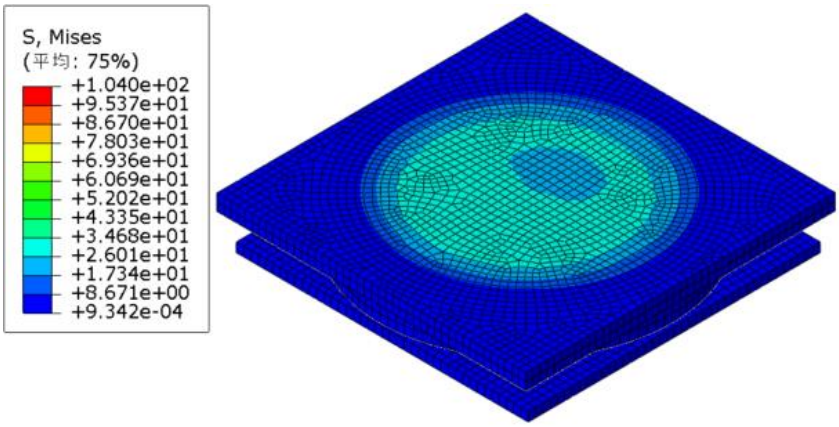

Fig. 6. Mises stress cloud

As can be seen from the figure, under the action of 1.2 times the design load, the maximum Mises stress is 104MPa, and all materials are in elastic state, which also reflects the correctness of the linear change of load-deformation curve and meets the design requirements(Feng 2020).

4.2 Modal Analysis

The purpose of modal analysis and calculation is to find out the natural frequency and main vibration mode of the structure. For an actual structure, there are many kinds of vibration frequencies and modes of each order. Because the high-order modes generally have little dynamic response to the structure, the lowest 3 to 5 modes are usually considered (Salunkhe et al. 2022).

Give each component the material parameters of its design material selection, and then carry out modal analysis on the established model. We calculated and analyzed the first 20 modes of the model, among which the 4th and 5th modes are more useful(Shang et al. 2021). The first order frequency is 267.8Hz and its vibration direction is vertical; The second-order frequency is 276.1Hz, and its vibration direction is the up-and-down movement direction. This vibration can cause the bearing to rotate. See Fig. 7 for the first-order and second-order modes. The mass damping of the structure with larger vibration frequency above the third order will weaken it.

4.3 Dynamic Analysis

In order to simulate the situation that the bearing encounters an earthquake in normal use, a surface load of 12500kN is applied to the upper surface of the bearing, and seismic waves are input at the bottom of the bearing (see Fig. 8) for analysis, and the distribution law of stress and strain of the bearing in the seismic load is obtained (Charki et al. 2013).

To analyze and study the dynamic response of the structure under the earthquake load, we mainly care about the strain of the main components of the bearing changing with time on the applied load spectrum (Peng et al. 2015). Among them, the curved PTFE plate and the spherical cap bushing are the main parts of the bearing, and we analyze the stress and strain as follows(Guo & Parker 2012).

Fig. 9 is the stress nephogram of the structural model at the peak. It can be seen from the figure that the stress distribution of the curved PTFE plate is uniform in the central part of the model, and its compressive stress distribution is between 7.5 MPa and 9.2 MPa; The maximum local stress at the edge is 14.5MPa, and the stress is less than the fiber stress of PTFE 45MPa, which meets the design requirements. The stress distribution in the center of spherical cap bushing is between 9 MPa and 22 MPa; The local maximum stress is about 62.8 MPa, and the stress is less than 375 MPa, which meets the design requirements.

Fig. 10 is the strain nephogram of the structural model at the peak. It can be seen from the figure that the strain of the curved PTFE plate changes uniformly in the horizontal direction, and the maximum vertical compressive strain is generated at the center of the structure, with the maximum compressive strain of 0.17 mm and the maximum circumferential strain of

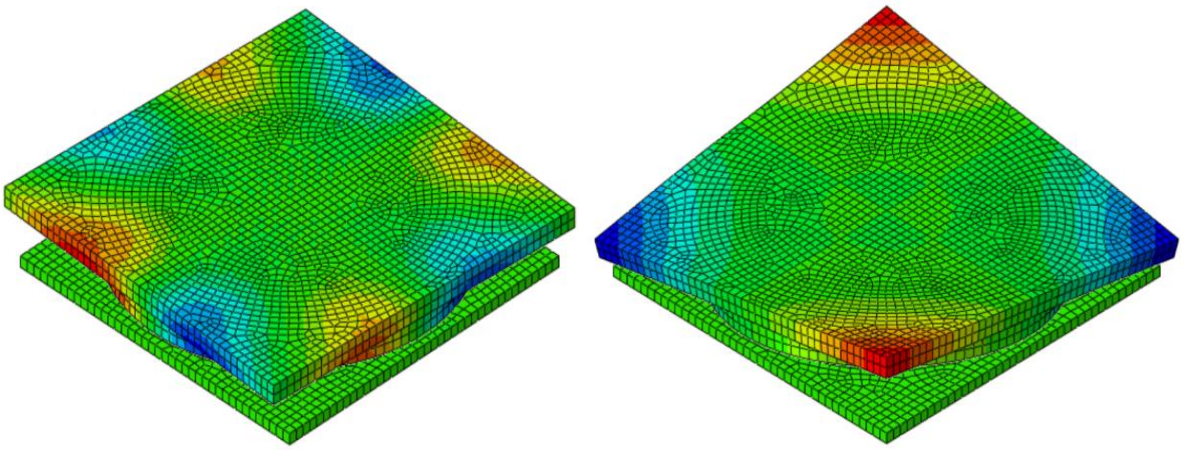

a 1 mode diagram **b 2 mode diagram**

Fig. 7. Vibration mode diagram of bearing

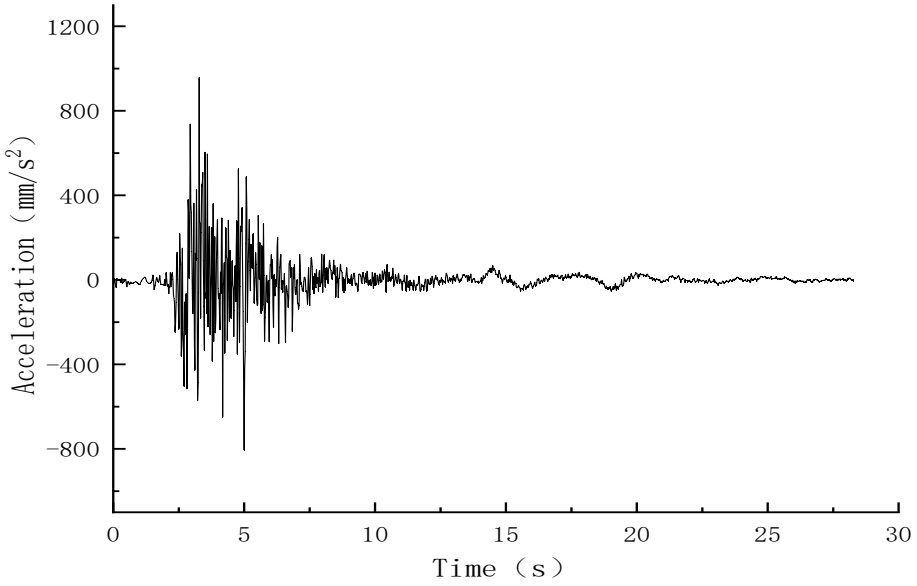

Fig. 8. Selected seismic waves

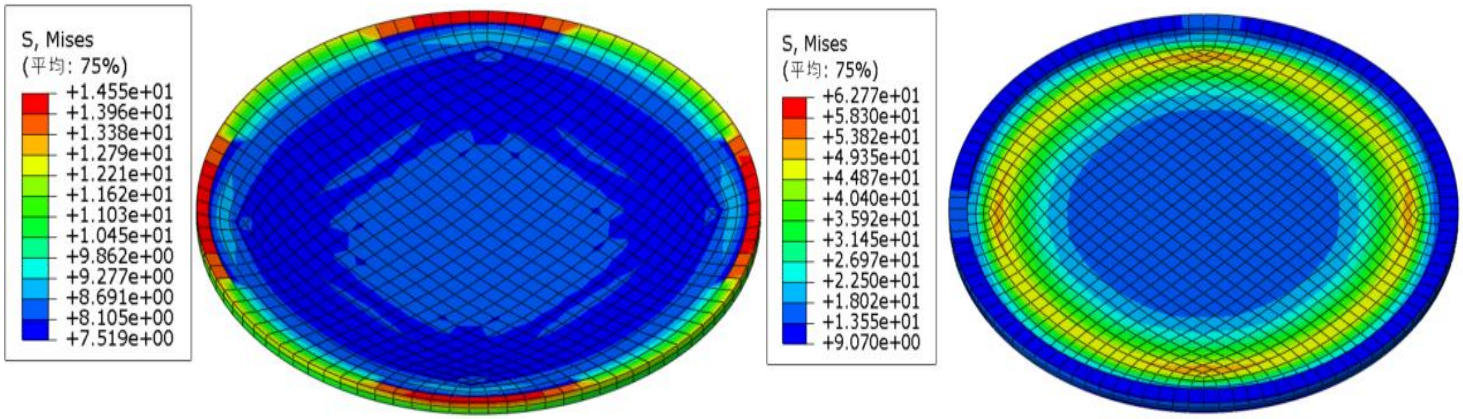

a Stress nephogram of curved PTFE plate b Stress nephogram of spherical cap bushing

Fig. 9. Model stress nephogram at the peak of earthquake acceleration

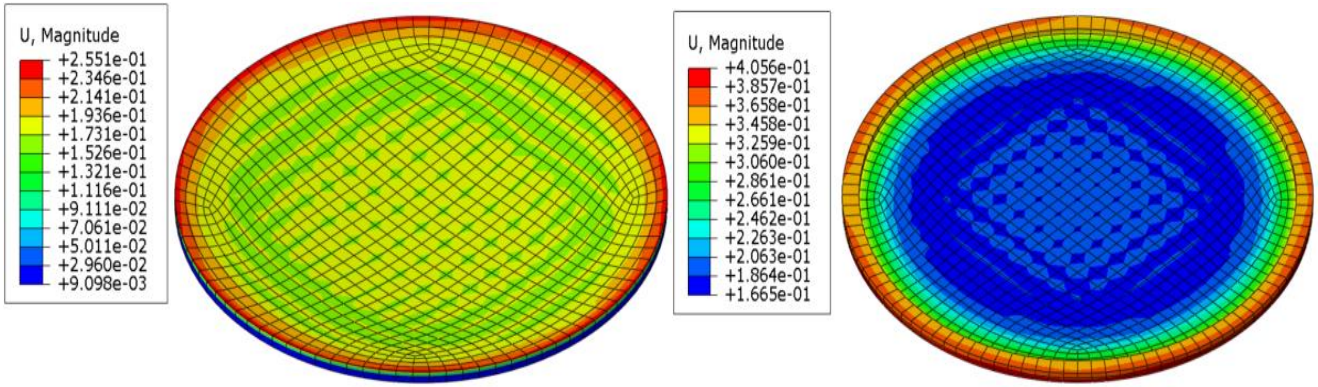

a Strain nephogram of curved PTFE plate b Strain nephogram of spherical cap bushing

Fig. 10. Model strain nephogram at the peak of earthquake acceleration

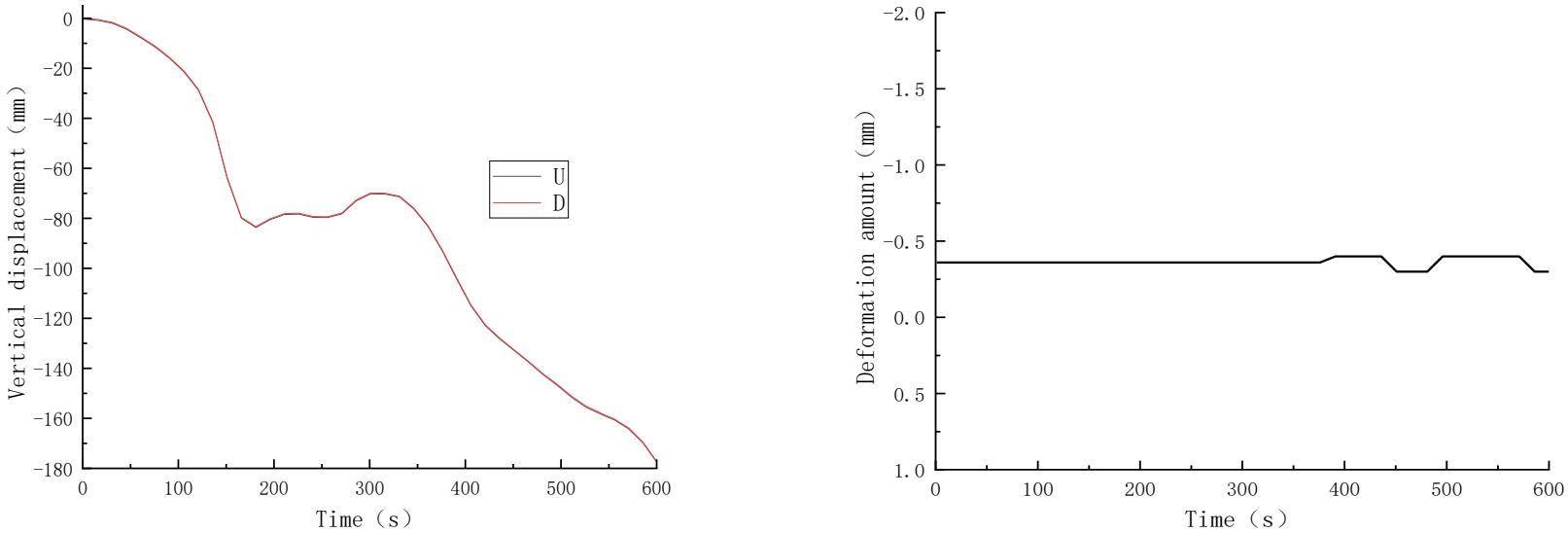

a DU curve displacement diagram **b DU curve difference diagram**

Fig. 11. Diagram of strain versus time

the model of 0.26 mm, and the deformation meets the design requirements. The maximum vertical compressive strain of spherical cap bushing is 0.23 mm, and the maximum circumferential strain is 0.41 mm, and the deformation meets the design requirements(Shen et al. 2011).

Select two points in the center of the upper and lower surfaces of the bearing, study the variation law of the strain of the bearing with time under the dynamic load (0~600s) at the peak section and draw its strain-time curve as shown in Fig. 11. Curve d in the figure is the vertical displacement-time curve of the center point of the lower surface of the support; U curve is the vertical displacement-time curve of the center point of the upper surface of the bearing (Cao et al. 2015).

The figure shows the vertical strain of the upper and lower surfaces of the bearing changing with time under dynamic load. It can be seen from the figure that due to the unequal strain of the upper and lower surfaces of the bearing, the bearing produces compression, and the maximum compression is 0.4 mm, which is 0.2% of the thickness of the bearing, and the compression deformation meets the design requirements (Dandagwhal & Kalyankar 2019).

5. CONCLUSION

In this paper, QZ12500GD seismic spherical bearing is analyzed. The static calculation, bearing modal analysis and dynamic analysis are carried out by Abaqus large-scale finite element analysis software, and the deformation and stress of the bearing are studied. It can be seen that the stress and strain of the main components meet the design requirements and the stress distribution of the main bearing components is uniform according to the relevant industry standards, which ensures the safety and reliability of the bearing. In the future, some scholars are interested in studying the effect of curvature on bearing capacity of curved polytetrafluoroethylene plate.

DISCLAIMER (ARTIFICIAL INTELLIGENCE)

Author(s) hereby declare that NO generative AI technologies such as Large Language Models (ChatGPT, COPILOT, etc.) and text-to-image generators have been used during the writing or editing of this manuscript.

COMPETING INTERESTS

Author has declared that no competing interests exist.

REFERENCES

Adamov, A. A., Kamenskikh, A. A., & Pankova, A. P. (2022). Influence analysis of the antifriction layer materials and thickness on the contact interaction of spherical bearings elements. *Lubricants, 10*(2), 30.

Ahmed, S. H., Al-Sarraj, G. I., & Abd, Z. M. (2024). Finite element analysis for cylindrical and balling bearings under static and dynamic loads: A review paper. *SVU-International Journal of Engineering Sciences and Applications, 5*(2), 109–118.

Cao, Q., Hua, L., & Qian, D. S. (2015). Finite element analysis of deformation characteristics in cold helical rolling of bearing steel-balls. *Journal of Central South University, 22*(4), 1175–1183.

Charki, A., Bigaud, D., & Guerin, F. (2013). Behavior analysis of machines and system air hemispherical spindles using finite element modeling. *Industrial Lubrication and Tribology, 65*(4), 272–283.

Ciubotariu, V. (2016). Nonconventional method of spherical roller bearing design, using FEA. *Revista de Tehnologii Neconventionale, 20*(3), 30.

Dandagwhal, R. D., & Kalyankar, V. D. (2019). Design optimization of rolling element bearings using advanced optimization technique. *Arabian Journal for Science and Engineering, 44*(9), 7407–7422.

Desavale, R. G., Venkatachalam, R., & Chavan, S. P. (2014). Experimental and numerical studies on spherical roller bearings using multivariable regression analysis. *Journal of Vibration and Acoustics, 136*(2), Article 021022.

Feng, J. W. (2020). Rich front approach span bearing finite element analysis of the large bridge. *Journal of Inner Mongolia Highway and Transport, 2020*(5), 36–38, 49.

Ghalamchi, B., Sopanen, J., & Mikkola, A. (2016). Modeling and dynamic analysis of spherical roller bearing with localized defects: Analytical formulation to calculate defect depth and stiffness. *Shock and Vibration, 2016*, Article 2106810.

Guo, Y., & Parker, R. G. (2012). Stiffness matrix calculation of rolling element bearings

using a finite element/contact mechanics model. *Mechanism and Machine Theory, 51*, 32–45.

Harris, T. A., & Kotzalas, M. N. (2006). *Advanced concepts of bearing technology: Rolling bearing analysis*. CRC Press.

McErlain, D. D., Milner, J. S., Ivanov, T. G., Jencikova-Celerin, L., Pollmann, S. I., & Holdsworth, D. W. (2011). Subchondral cysts create increased intra-osseous stress in early knee OA: A finite element analysis using simulated lesions. *Bone, 48*(3), 639–646.

Mohamed Anwar, A. U., Babu, S., & Starvin, M. S. (2024). Experimental validation and contact behaviour analysis of slewing ring thrust ball bearings with FEA simulation. *Sādhanā, 49*(4), 267.

Peng, X., Wu, C. L., & Chen, Z. H. (2015). A finite element analysis on hybrid UHMWPE pads of a spherical bearing. *Materials Research Innovations, 19*(Suppl. 8), S8-229.

Salunkhe, V. G., Desavale, R. G., & Kumbhar, S. G. (2022). Vibration analysis of deep groove ball bearing using finite element analysis and dimension analysis. *Journal of Tribology, 144*(8), Article 081202.

Shah, D. B., Patel, K. M., & Trivedi, R. D. (2016). Analyzing Hertzian contact stress developed in a double row spherical roller bearing and its effect on fatigue life. *Industrial Lubrication and Tribology, 68*(3), 361–368.

Shang, J., Yin, B., Du, Z., et al. (2021). Spherical bearing in the process of FPSO construction train application. *Journal of Chemical Industry in Shandong, 50*(19), 190–191, 193.

Shen, Y., Fan, Z., & Zhang, P. (2011). Design and analysis of spherical bearings in building structures. *Steel Structure, 26*(6), 6–11.

Wang, S. B., Zhang, X. Z., Wu, K., & Sun, Y. (2011). Finite element analysis for belt conveyor's drum. *Advanced Materials Research, 228*, 764–770.

Xue, Y., Chen, J., Guo, S., Meng, Q., & Luo, J. (2018). Finite element simulation and experimental test of the wear behavior for self-lubricating spherical plain bearings. *Friction, 6*(3), 297–306.

Peer-review history:
The peer review history for this paper can be accessed here:
https://www.sdiarticle5.com/review-history/128454